2013

A Novel Method for Prediction of Mobile Robot Maneuvering Spaces

Patrick N. Currier
Embry-Riddle Aeronautical University, currierp@erau.edu

Alfred L. Wicks
Virginia Polytechnic Institute and State University

https://doi.org/10.1016/j.jterra.2013.03.001

A NOVEL METHOD FOR PREDICTION OF MOBILE ROBOT MANEUVERING SPACES

Patrick N. Currier[a1*] and Alfred L. Wicks[b]

[a]*Virginia Polytechnic Institute and State University – Dept. of Mechanical Engineering – 114 Randolph Hall, Blacksburg, VA USA 24061*

[b]*Virginia Polytechnic Institute and State University – Dept. of Mechanical Engineering – 114 Randolph Hall, Blacksburg, VA USA 24061 – awicks@vt.edu*

Abstract

As the operational uses of mobile robots continue to expand, it becomes useful to be able to predict the admissible maneuvering space to prevent the robot from executing unsafe maneuvers. A novel method is proposed to address this need by using force-moment diagrams to characterize the robot's maneuvering space in terms of path curvature and curvature rate. Using the proposed superposition techniques, these diagrams can then be transformed in real-time to provide a representation of the permissible maneuvering space while allowing for changes in the robot's loading and terrain conditions. Simulation results indicate that the technique can be applied to determine the appropriate maneuvering space for a given set of loading conditions, longitudinal acceleration, and tire-ground coefficient of friction. This may lead to potential expansion in the ability to integrate predictive vehicle dynamics into autonomous controllers for mobile robots and a corresponding potential to safely increase operating speeds.

Keywords: mobile robots, maneuvering spaces, predictive dynamics

[1] *Embry-Riddle Aeronautical University – Dept. of Mechanical Engineering – 600 S. Clyde Morris Blvd, Daytona Beach, FL USA 32114 –Email: currierp@erau.edu*

[*] *Corresponding Author*

1 Introduction

This work proposes a methodology for real-time prediction of the dynamic operating envelope of a large mobile robot. The method abstracts a vehicle model of arbitrary complexity using a force-moment representation that can then be transformed into an operating manifold expressed in terms of motion variables to outline vehicle performance limitations. Additionally, the method allows for realistic variation in vehicle Center of Gravity (CG), longitudinal acceleration, and terrain surface conditions as represented by a coefficient of friction.

1.1 Background

Large scale robotic demonstrations such as the DARPA Grand Challenges have demonstrated the potential inherent in applying autonomous technologies to large mobile robots operating at high speed over uncertain terrain. In these conditions, the dynamics of the vehicle can become highly significant to the ability of the robot to safely maneuver and failures modes, such as roll-over, that can be largely overlooked in smaller rovers can have catastrophic consequences. To avoid this type of failure, shown in Fig 1, it is necessary for an autonomous controller to have the ability to predict and compensate for the dynamic limits of the vehicle [1].

Fig. 1: *Rollover of large mobile robot due to an attempted maneuver beyond the vehicle's dynamic limits.*

Despite evidence of this need, many current autonomous controllers rely on simple kinematic models to define vehicle limitations in the planning and execution stages of control [2]. The kinematic, bicycle model is widely used due to ease of implementation and, when implemented with an appropriate understeer coefficient, reasonable accuracy in predicting motion of the class of Ackerman-steered vehicles that are commonly used for large mobile robotics [3]. The bicycle model compresses the two wheels on each axle of a vehicle into a single track, and is thus unable to account for the non-linear effects of lateral normal force transfer that can significantly affect the handling dynamics of a vehicle [4][5]. These kinematic models are generally adequate for defining the non-holonomic motion constraints, but may allow for trajectories that are non-admissible due to dynamic constraints to be considered and executed [6].

Additionally, most high-level planning work to date relies on the assumption that the vehicle and terrain conditions are invariant, particularly in regards to vehicle load the tire-ground

coefficient of friction [7]. Several techniques have been developed to estimate these important quantities based on measurements of vehicle state. These techniques, however, stop short of integrating these estimates into mobile robot planning [8][9][10][11][12].

2 Methods

One of the primary potential advantages of autonomous controllers on mobile robots is the ability to use feed-forward controllers to avoid potentially dangerous situations instead of attempting to compensate with feedback. In order to allow this use, it is necessary to create a function that can map the feed-forward control inputs to the predicted dynamic state output. For the class of four-wheeled, Ackerman-steered mobile robots considered in this work, the control inputs are the steering angle of the front wheels and the torque at the wheels as dictated by the drive and/or brake settings. The outputs are the motion variables; these will be defined as a path curvature, curvature rate, longitudinal velocity, and longitudinal acceleration.

An accurate dynamic vehicle model must consider a very large number of effects; a multibody commercial dynamic model such as VehicleSim may include more than 200 degrees-of-freedom [13]. Due to the complexity of the factors involved when dynamic effects are considered, it becomes difficult to derive a tractable closed-form solution to the desired feed-forward function. Additionally, many autonomous controllers rely on search techniques to determine an optimal path from a candidate space. These techniques require the feed-forward function to be supply an entire space of admissible trajectories in real-time and not just a single solution.

The proposed method uses a numerical solver to precalculate the motion variable outputs from a vehicle model across the entire potential maneuvering space. These results can be stored and then accessed in real-time by the feed-forward controller by applying superposition techniques based on the current state of the vehicle.

2. 1 Modeling Technique

To simplify the vehicle model into a form that can be stored, a quasi-static force-moment representation is used. This method, championed by Milliken represents the maneuvering state of the vehicle in terms of lateral and longitudinal forces and yawing moments, as illustrated in Fig. 2 [14]. The searchable operating space can be characterized in coordinates of the lateral slip angles at the front and rear wheels. The force-moment diagram can be solved numerically across the searchable space for the lateral force, longitudinal force, and yawing moment.

This representation has the effect of abstracting the specifics of the actual vehicle model from the remainder of the method. A vehicle model of arbitrary complexity can be used, provided that it can be solved for the appropriate coordinates and variables. Using numerical solution

techniques, it is therefore possible to build a quasi-static map of the vehicle performance while taking the highly non-linear aspects of components such as tires in to account.

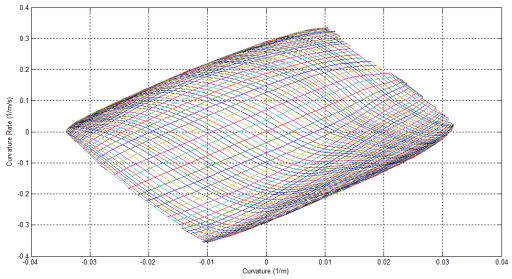

Fig. 2: *Example of a manuever space in terms of path curvature versus curvature rate at a constant longitudinal force across the space of front and rear slip angles.Each line with a negative slope represents a constant front wheel steering angle and each line with a positive slope indicates a constant body slip angle.*

For purposes of this work, a relatively simple (when compared to a multi-body commercial system) model incorporating lateral and longitudinal load transfer and a combined-slip, non-linear Fiala tire model was implemented in MATLAB. The model is based on the simplified 4-wheel representation formulated by Will and Zak and was selected as the simplest representation capable of capturing the critical sprung mass weight transfer response to accelerations [15]. The model has a total of 11 degrees of freedom: translation in the *x*, *y*, and *z* body-fixed vehicle axes, rotation of the vehicle about the *z*-axis ( ), rotation of the sprung mass about the *x*-axis ( ), rotation of the sprung mass about the *y*-axis ( ), steering of the front wheels ( ), rotation of each individual wheel ( ), and location of the sprung mass center of gravity relative to the body-fixed vehicle axes ( ). The model is assumed to have a known CG location that may be variable within bounds due to the effects of payloads (such as cargo) carried by the vehicle. The vehicle frames are shown in Fig. 3.

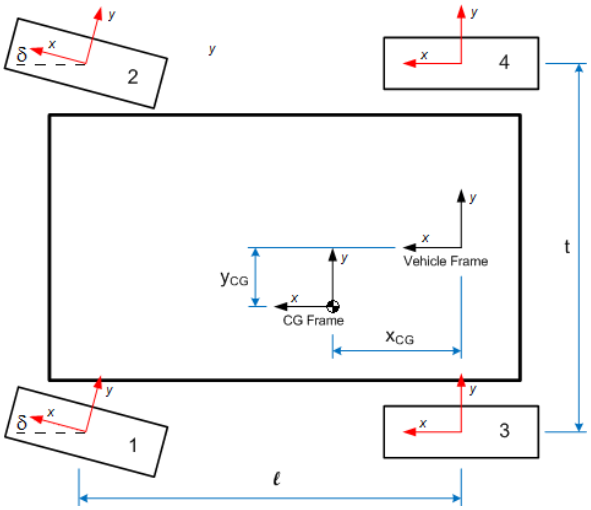

Fig. 3: *Vehicle coordinate frames showing location of vehicle frame at the center of the rear axle and its relationship to the CG and wheel frames.*

During maneuvering of a standard vehicle, assumed for purposes of this work to be a 4-wheeled vehicle with suspended wheels and front-wheel steering, significant weight transfers can and will occur in response to lateral (*y*-axis) and longitudinal (*x*-axis) accelerations. These weight transfers can be modeled as acting through the roll centers of the suspension, which are defined as the point at which a lateral force applied to the sprung mass does not create a rolling moment [14]. The roll centers are determined kinematically and can move in response to suspension jounce, but this movement is assumed to be small and neglected for this model. Suspension effects can be generalized and separated into orthogonal components by modeling the connection between the sprung and unsprung masses as a revolute joint placed at each roll center oriented along the roll axis and an additional joint oriented parallel to the vehicle *y*-axis at the pitch center.

Assuming that the vehicle is operating on a roughly planar surface, the longitudinal portion of the weight transfer (ΔW_{x_N}) at axle *N* will occur primarily due to throttle and brake inputs and can be modeled by taking moments about the contact patches [14]:

$$\Delta W_{x_F} = -\frac{1}{\ell}(z_{CG} + R_e) g m_s A_x \qquad (1)$$

$$\Delta W_{x_R} = \frac{1}{\ell}(z_{CG} + R_e) g m_s A_x \qquad (2)$$

where *g* is the acceleration due to gravity, R_e is the effective rolling radius of the wheels, m_s is the mass of the sprung body, A_x is the longitudinal acceleration due to throttle or brake input, and ℓ is the effective wheelbase.

Lateral weight transfer occurs primarily due to the lateral accelerations acting on the CG during turning maneuvers. The roll axis defined by the roll centers causes this to be governed by a characteristic height (*H*) that is the Euclidean distance between the CG and the roll axis at the longitudinal location of the CG:

$$H = z_{CG} + R_e - \frac{1}{\ell}\left(z_{RC_F} x_{CG} + z_{RC_R}(\ell - x_{CG})\right) \qquad (3)$$

where z_{RC_N} represents the height of the roll center of axle *N* relative to the vehicle frame. This height can then be used to derive the effect of lateral acceleration (ΔW_{y_N}) by taking moments about one side of the vehicle, as shown by Milliken [14]:

$$\Delta W_{y_N} = \frac{k_{\phi_N} m_s g A_y H}{t_F\left(k_{\phi_F} + k_{\phi_R} - m_s g A_y y_{CG} - m_s g H\right)} + m_s g A_y \frac{\Lambda_N x_{RC_N}}{\ell t_N} \qquad (4)$$

where k_{ϕ_N} is the effective roll stiffness of axle *N*, t_N represents the track width of the axle *N*, and $\Lambda_F = x_{CG}$ or $\Lambda_R = \ell - x_{CG}$. Additional weight transfer from the nominal values may occur due to lateral CG offsets. This can be calculated using a normalized coefficient for each wheel *n* (C_{y_n}) [14]:

$$C_{y_n} = \frac{1}{2} + sign(y_{CG})\frac{y_{CG}}{0.5t_N}. \qquad (5)$$

The total instantaneous weight distribution (F_{z_n}) can then be found by calculating the static weight distribution (F_{s_n}) and superimposing the dynamic effects:

$$F_{s_n} = \frac{1}{\ell} C_{y_n} m_s g \Lambda_N + m_u g \qquad (6)$$

$$F_{z_n} = F_{s_n} + \Delta W_{y_N} + C_{y_n} \Delta W_{x_N} \qquad (7)$$

to yield the total expected normal force on each wheel.

Once the effects of the weight distribution have been calculated, the normal force can be used as an input to a combined-slip tire model to calculate the lateral and longitudinal forces at the ground that actually determine vehicle motion. The Fiala model characterizes tire tractive response in terms of the physically recognizable parameters of normal force (F_{z_n}), tire slip angle (α_n), tire slip ratio (S_n), overall cornering stiffness (C_α), traction coefficient (C_s), and effective coefficient of friction (μ). This model can be derived from a brush tire model and is valid for combined-slip conditions involving simultaneous longitudinal and lateral accelerations. Most simplified models, such as the commonly used lateral bicycle representations neglect the effects of longitudinal force generation. This effect can be particularly important in low friction conditions, as tires are only capable of generating a maximum amount of force that must be distributed between longitudinal acceleration and turning.

The form of the Fiala model used in this work is taken from Hsu and can be represented by [12]:

$$F_{x_n} = C_s \left(\frac{S_n}{1+S_n}\right)\frac{F}{f} - C_{rr} F_{z_n} \qquad (8)$$

$$F_{y_n} = C_\alpha \left(\frac{\tan \alpha_n}{1+S_n}\right)\frac{F}{f} \qquad (9)$$

where

$$F = \begin{cases} f - \frac{1}{3\mu F_{z_n}} f^2 + \frac{1}{27\mu^2 {F_{z_n}}^2} f^3, & f \le 3\mu F_{z_n} \\ \mu F_{z_n}, & f > 3\mu F_{z_n} \end{cases} \qquad (10)$$

and

$$f = \sqrt{{C_s}^2 \left(\frac{S_n}{1+S_n}\right)^2 + {C_\alpha}^2 \left(\frac{\tan \alpha_n}{1+S_n}\right)^2} \qquad (11)$$

Note that the longitudinal force equation is augmented by a term $C_{rr} F_{z_n}$ that represents the rolling resistance of the tire. A full derivation of this model can be found in Pacejka [16].

From the tire model, the contribution of each wheel to the total lateral (F_y) and longitudinal (F_x) forces acting on the vehicle can be determined. These forces can thus be summed in the vehicle frame after correcting for the steering angle (δ_N):

$$F_x = \sum_{n=0}^{4} F_{x_n} \cos\delta_N + F_{y_n} \sin\delta_N \qquad (12)$$

$$F_y = \sum_{n=0}^{4} F_{x_n} \sin\delta_N + F_{y_n} \cos\delta_N \qquad (13)$$

The overall yawing moment (M) about the vehicle frame can be determined by summing the cross products of the resultant vector wheel forces (F_n):

$$M = \sum_{n=1}^{4} p_n \times F_n \qquad (14)$$

where p_n is the position vector from the vehicle frame origin to the center of wheel n.

This non-linear model was numerically solved in terms of the coordinates of steering angle (δ) and body slip angle (β) using a *trust-region-dogleg* algorithm implement in the MATLAB function *fsolve* to find the resultant lateral force and yawing moment over the grid of angular coordinates for a fixed longitudinal force to create a set of force-moment diagrams. The values in the diagrams were then non-dimensionalized using the weight and wheelbase of the vehicle as the normalizing terms to form a lateral force coefficient C_Y and a yawing moment coefficient C_M.

For purposes of navigation and control, a representation of vehicle performance in terms of motion variables is desirable, necessitating a transformation from force-moment coordinates to path curvature, curvature rate, and acceleration. Since the knowledge of the state of these variables allows for prediction of the future path of the vehicle, this defines a "maneuver space" consisting of the set of achievable path variables. A vehicle operating at a point within this space with a zero curvature rate will trace a path of a circle with a radius equal to the inverse of the path curvature while a vehicle with a non-zero curvature rate will trace a path of increasing or decreasing radius. The edges of the space indicate the limits of vehicle performance, i.e. the largest path curvature contained within the space represents the minimum achievable turning radius, even if this minimum radius may not be sustainable at steady state (as indicated by a non-zero curvature rate).

Assuming a current or desired longitudinal velocity is known, the path curvature can be calculated by assuming that all of the lateral force is used to offset the centripetal force due to curvilinear motion [14]:

$$\kappa = \frac{C_Y g}{{V_x}^2} \qquad (15)$$

where κ is the instantaneous vehicle path curvature or the inverse of the turning radius and V_x is the longitudinal speed in the direction of the vehicle frame x-axis.

An expression can then be derived to relate the yawing moment to a rate of change of curvature:

$$\frac{M}{I_z} = \frac{C_N W \ell}{I_z} = \ddot{\theta} = \frac{d}{dt}(V_x \kappa) \qquad (16)$$

$$\frac{C_N W \ell}{I_z} = \dot{V}_x \kappa + V_x \dot{\kappa} \qquad (17)$$

$$\dot{\kappa} = \left(\frac{C_N W \ell}{I_z} - \dot{V}_x \kappa\right) \frac{1}{V_x} \qquad (18)$$

where $\dot{\kappa}$ is the instantaneous rate of change of curvature and I_z is the moment of inertia about the z-axis. In many cases the exact moment of inertia is unknown but can be approximated using the dynamic index [17]:

$$DI = \frac{{r_z}^2}{x_{CG}(\ell - x_{CG})} \qquad (19)$$

where r_z is the radius of gyration of the vehicle. For most vehicles, the dynamic index is approximately equal to unity, with slightly lower values found on high performance vehicles [17]. The moment of inertia is related to the dynamic index by:

$$I_z = m_s x_{CG}(\ell - x_{CG}) DI \qquad (20)$$

and can thus be reasonably approximated for most vehicles using knowledge of the mass of the sprung body and the location of the CG.

Once the curvature coordinates have been transformed, it becomes useful to transform the slip angles into the more useful coordinates of the front wheel steering angle and body slip angle. Kinematics can be used to derive an expression for the steering angle [14]:

$$\delta = atan(\ell \kappa) + \alpha_r - \alpha_f \qquad (21)$$

Since the commonly used navigation frame is located at the center of the rear axle, transformation of the rear slip angle to the body slip angle is trivial in a front-steer only vehicle. Provided that the solution grid is dense enough, these angular transformations can be performed by linear interpolation.

2.2 Parameter Variation

An important aspect of this work is the ability to account for temporal variations in both vehicle load and terrain conditions. In order to do this, it is necessary to have an estimate of the current values of these parameters. Estimation of these values is beyond the scope of this work, but techniques are further developed in [18].

Assuming that the load state of the vehicle can be estimated, it becomes necessary to define a method for incorporating that knowledge into estimates of the maneuvering space. To do this, the load state of the vehicle can be defined in terms of the mass of the vehicle and the location of the

CG relative to the navigation frame in three dimensions. This definition assumes that the CG location of a typical vehicle in its empty state can be known and that changes in CG are likely to be affected mainly by the addition of cargo or passengers. Furthermore, it is assumed that the parameters of the load state can be reasonably bounded based on known vehicle characteristics.

An example of this would be a pickup truck with a rear bed. The location of the CG of the pickup truck when carrying no bed load, fuel, or passengers can generally be known. This state is considered the "empty" load state of the vehicle. As passengers and cargo are added, the total vehicle CG location will change in response to the added mass. On a vehicle such as a pickup truck, it is reasonable to place bounds on the mass based on the rated capacity of the truck and on the CG location by making assumptions as to likely locations of this mass (i.e. the *x* location of the CG is likely to shift farther in the direction of the cargo bed than in the direction of the cab). Although techniques for doing so are beyond the scope of this paper, it is possible in many cases to measure, estimate, or input parameters to allow for calculation of the current load state based on the current cargo configuration.

Using the techniques developed in the previous section, it is possible to precalculate the maneuvering space of the vehicle for any arbitrary location of the CG. Conveniently the mass can be factored out of the equations and is not necessary if the CG location is known. The obvious difficulty with this technique is that it is usually infeasible to precalculate maneuvering space maps for all possible (or even all likely) CG locations as the number of combinations becomes intractable for even coarse discretizations due to the potential variation in three dimensions.

This difficulty can be addressed by the simple realization that the maneuvering characteristics of the vehicle are determined by the forces and moments acting on the body; these forces and moments have already been approximated by the numerical solution technique. It is therefore possible to decouple the three dimensional variation and precalculate the effect of movement of the CG in any one dimension on the resultant forces. These effects can be calculated over a relatively small number of cases represented by a discretization of likely CG locations.

Using the pickup truck example, the resultant forces would first be calculated for the empty truck using the known CG location. By applying domain knowledge, a set of likely x_{CG} locations can be formulated and the resultant forces that would occur in this load state can be calculated. For the pickup truck, this set would likely include a small number of values of CG location forward of the empty CG (assuming only passengers) and a larger number of values to the rear of the empty CG location (assuming heavy cargo). This procedure can be repeated for the decoupled y_{CG} and z_{CG} parameters. If a set of size 10 is used for each variable, this would require calculation of 30 loaded cases plus the empty case. If these sets are not decoupled, this would require calculation of approximately 1000 independent load cases, which would be much more expensive in terms of computation and storage of results.

The results of the computation of the decoupled load cases are a set of predicted lateral forces and yawing moments expressed in terms of the non-dimensionalized coefficients C_Y and C_M. Although the couplings between load states with different 3D CG locations are non-linear, when the resultant effects are expressed in terms of forces and moments, it becomes possible to linearly interpolate the results of the decoupled solutions and achieve a reasonable estimate of the uncalculated coupled solution:

$$Y = Y_{empty} + \left(Y_{x_{loaded}} - Y_{empty}\right) + \left(Y_{y_{loaded}} - Y_{empty}\right) + \left(Y_{z_{loaded}} - Y_{empty}\right) \quad (22)$$

$$M = M_{empty} + \left(M_{x_{loaded}} - M_{empty}\right) + \left(M_{y_{loaded}} - M_{empty}\right) + \left(M_{z_{loaded}} - M_{empty}\right) \quad (23)$$

where the subscript *empty* indicates the force or moment result produced by the unloaded vehicle case and the subscript *loaded* indicates the result produced by the decoupled CG offset case. For example, if the location of the loaded CG were determined to be simultaneously offset from the empty CG by 0.1m in the *x* direction, 0.05m in the *y* direction, and 0.2m in the *z* direction, the *loaded* terms would consist of the results from the precalculated cases of a 0.1m *x* offset (assuming empty case *y* and *z* locations), of a 0.1m *y* offset (assuming empty case *x* and *z* locations), and of a 0.1m *z* offset (assuming empty case *x* and *y* locations). The output of Eqs. 22-23 would represent the estimate of forces produced by the 3D dimensional offset without the need to directly calculated the coupled result. It can also be seen by inspection that Eqs. 22-23 can be reduced to:

$$Y = -2Y_{empty} + Y_{x_{loaded}} + Y_{y_{loaded}} + Y_{z_{loaded}} \quad (24)$$

$$M = -2M_{empty} + M_{x_{loaded}} + M_{y_{loaded}} + M_{z_{loaded}} \quad (25)$$

The resultant superimposed forces and moments can then be transformed using Eqs. 15-18 to yield an estimate of the maneuvering space for the vehicle in the load condition represented by the offset CG. If a higher fidelity for load cases between the discretizations is desired, it is also possible to linearly interpolate for any value of CG coordinates between the precomputed discretizations.

2.2 Friction and Acceleration Effects

Another important characteristic that determines vehicle performance capabilities is the ability of the tire to produce force due to its contact with the terrain surface. Without delving into the intricacies of terramechanics, variations in the terrain conditions can be largely characterized in terms of the tire ground coefficient of friction. Changes in the friction coefficient can have an enormous impact on the available maneuvering space for a mobile robot. Any driver who has ventured onto black ice on a highway and lost control of his or her vehicle can likely verify this claim. This effect results from the reduction of the total amount of force generation capability available to the tire, a number that can be grossly represented as the product of the coefficient of friction and the normal force. As the coefficient of friction decreases, the tires can no longer

produce enough force to hold the vehicle on the desired trajectory against the effects of inertial and centripetal forces.

As can be noted from the references cited previously, estimation of the friction coefficient in real-time and in realistic driving conditions is a decidedly non-trivial undertaking. Accuracy tends to be low and precision is largely determined by the level of excitation in the system. As a result, it is logical to partition the friction space into a small, discrete number of bins, as shown in Table 1, for purposes of integration into a maneuvering space mapping algorithm.

Table 1: Friction space partitions

Coefficient Range	Likely Terrain Surface
0.75-1.0	Dry paved road
0.50-0.75	Wet paved road or hard unpaved road
0.25-0.50	Soft unpaved road or snow
0.0-0.25	Wet mud or ice

As changes in the friction coefficient with this coarse discretization tend to have far more significant effects on the resulting force-moment diagram than changes in CG location, it becomes difficult to achieve good results by applying the type of superposition used for CG variation. However, it is possible to exploit the coarse binning of the friction coefficient by simply calculating the resultant forces for each friction bin. This approach would be computationally intractable without the proposed superposition algorithm as even the limited partition of the friction space requires a four-fold increase in computation time. The reduced number of computational cases, O^1 versus O^3, required by the decoupling of CG variables enables this the be a feasible approach.

An often neglected aspect of vehicle performance in navigation algorithms is the effect of longitudinal acceleration on the maneuver space. The total amount of force available from the tires is limited by the normal forces and coefficient of friction. Any force required to longitudinally accelerate the vehicle is thus not available to produce a lateral path change. This effect is often referred to as the friction ellipse [14]. Intuitively, this makes sense as a vehicle under heavy braking will tend to slide when a turn that could normally be executed is attempted. This problem is particularly relevant to autonomous systems as rapid turn maneuvers are typically only needed in emergency situations such as obstacle avoidance when the vehicle is also likely to be braking.

Similarly to the coefficient of friction, this effect can be handled by partitioning the acceleration cases into a limited set of acceleration values. The exact values used would depend on the capabilities of the vehicle but a set such as: steady-state road load, hard braking, moderate

braking, hard throttle is suggested. This further increases the computational complexity of the precalculations. To account for both friction and acceleration effects the number of precalculated cases required becomes:

$$\#\ cases = (\#\ \mu\ cases)(\#\ A_x\ cases)(\#\ x_{CG}\ cases + \#\ y_{CG}\ cases + \#\ z_{CG}\ cases) \quad (26)$$

When bounded by reasonable domain knowledge, the size of the result of Eq. 26 can be controlled will almost always be much smaller than the required number of cases for calculation all possible permutations of friction, acceleration, and CG location.

3. Results

To show the effect of the developed methodology, a model of a small rear-wheel drive truck was implemented in MATLAB and tested against a multi-body representation of the same vehicle using Mechanical Simulation's TruckSIM package.

To test the accuracy of the force-moment modeling technique, the TruckSIM model was driven with the integrated driver model over a 3km road course to generate a set of control inputs. These control inputs were then fed into an open-loop Simulink simulation using the force-moment model and the resultant trajectories are shown in Fig. 4. As can be seen in Table 2, the Simulink simulation, despite running in pure open-loop mode produced mean relative path errors (path error per total distance traveled) of 5% or less.

Table 2: Force-moment simulation results

Name	Velocity	μ	% Error
Case 1	30 kph	1.0	3.8%
Case 2	Varying 20-50 kph	1.0	5.0%
Case 3	50% of Case 2	1.0	4.4%
Case 4	50% Throttle	1.0	1.7%
Case 5	30 kph	0.5	3.5%

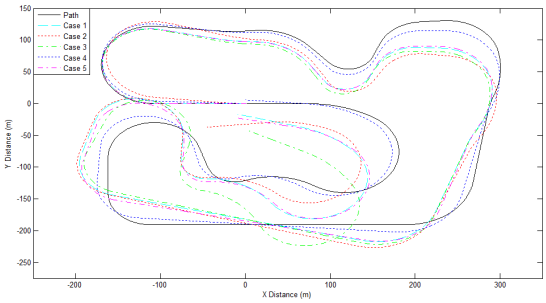

Fig. 4: *Results of simulation using force-moment model with CG variation as given by Table 2. Note that although the simulation was run purely open loop, the desired trajectory is acccurately recreated.*

To demonstrate the need for an adaptive model in terms of load condition, a similar set of runs was executed using CG heights and masses that were intentionally set to values different from that of the TruckSIM model, as shown in Table 3. As can be seen in Fig. 3, variations of the CG height and vehicle mass of the force-moment model from the nominal configuration produce differing simulation tracks. These results indicate that more advanced knowledge of the actual load state of the vehicle would be beneficial to increase accuracy of the model predictions, although the effect is small in this case. The small magnitude of the effect is likely exacerbated by the relative insensitivity of the vehicle to changes in CG height, as shown in Fig. 8. Further testing involving variation of additional parameters and testing involving a live vehicle with varying CG appears to be warranted in order to confirm these results.

Table 3: CG variation parameters results

Name	CG Height	Mass	Relative Path Error
Case 1 (nominal)	0.50m	1000kg	5.3%
Case 2	0.75m	1000kg	5.2%
Case 3	0.50m	1500kg	7.4%
Case 4	0.75m	1500kg	5.1%
Case 5	0.50m	2000kg	7.5%
Case 6	0.75m	2000kg	7.2%

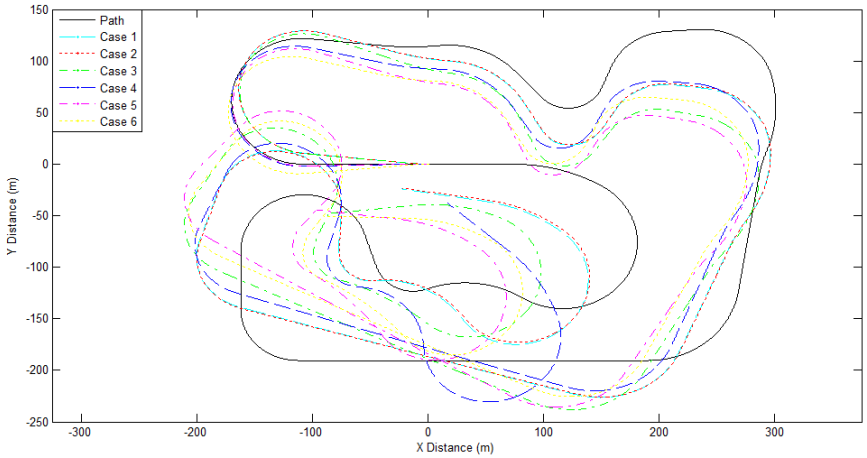

Fig. 5: *Results of simulation using force-moment model with CG variation as given by Table 3. Note the divergence in the path tracks compared to the results of Fig. 4 as parameters are varied from nominal.*

3.1 CG Location Variation & Superposition

The effect of variations in decoupled CG position as loading conditions change can be demonstrated by calculating the maneuvering manifold for a set of varying parameters ranging from a positive 0.1m offset to a negative 0.5m offset. As shown in Fig. 6, variation of produces a significant change in the maneuvering space. The available curvature rate increases

size but the vehicle becomes less stable as indicated by the peaks of the plot crossing into the negative curvature half-plane. This can be classified as an oversteer condition and would be expected as the CG is shifted aft in the vehicle. A forward shift in CG results in a decrease in curvature rate and an increase in more stable understeer behavior.

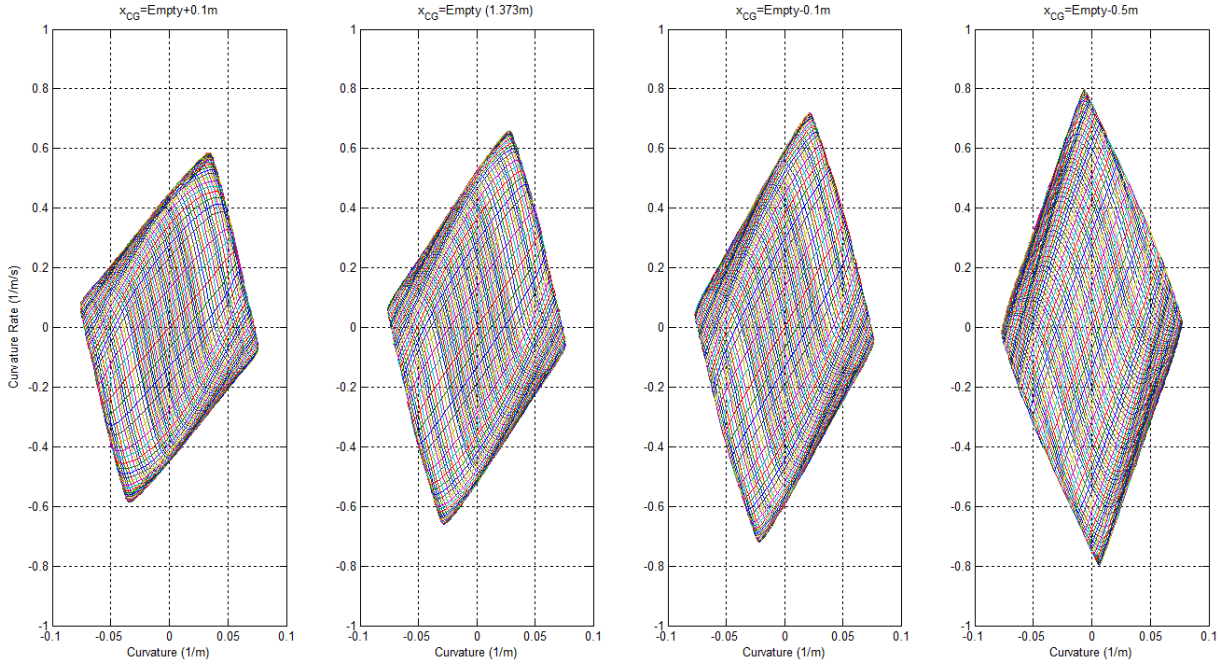

Fig. 6: *Plot of manuevering space diagrams showing the effect of variaiton of the x position of the CG. Note that the vehicle tends to oversteer (the peaks of the plot cross the curvature axis) as the CG shifts rearward.*

The vehicle was also simulated over a range of values for CG variation in the *y* and *z* directions. The CG was shifted by a magnitude of 0.3m in each direction on the *y*-axis and over a range from negative 0.1m to 0.4m in the *z*-axis. As can be seen in Fig. 7-8, the vehicle showed a small sensitivity to shifts in both axes. The diagram shows slight deformation near the handling boundaries, but the overall effect is minimal. This result is not entirely unexpected, as the CG location in these axes does not tend to have a large impact on the understeer/oversteer characteristics of a vehicle [14].

A much larger impact due to variations in these axes is seen in terms of the rollover tendencies. Although not discussed in this paper, this technique can be extended to calculation of dynamic stability indices. These indices show large and significant changes as a result of CG variation in the *y* and *z* axes. Further discussion of this phenomenon can be found in [18].

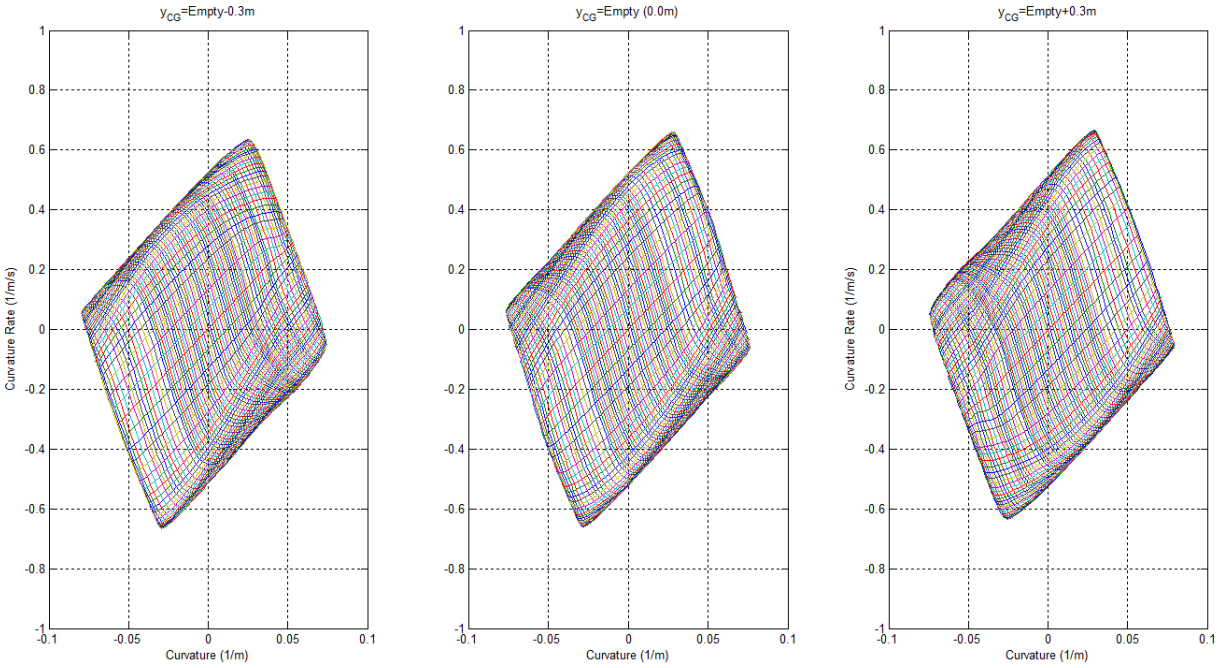

Fig. 7: *Plot of manuevering space diagrams showing the effect of variaiton of the y position of the CG. Note that the vehicle is largely insensitive to variation in this parameter in terms of manuevering space, although some effect is seen near the upper and lower bounds of the plot.*

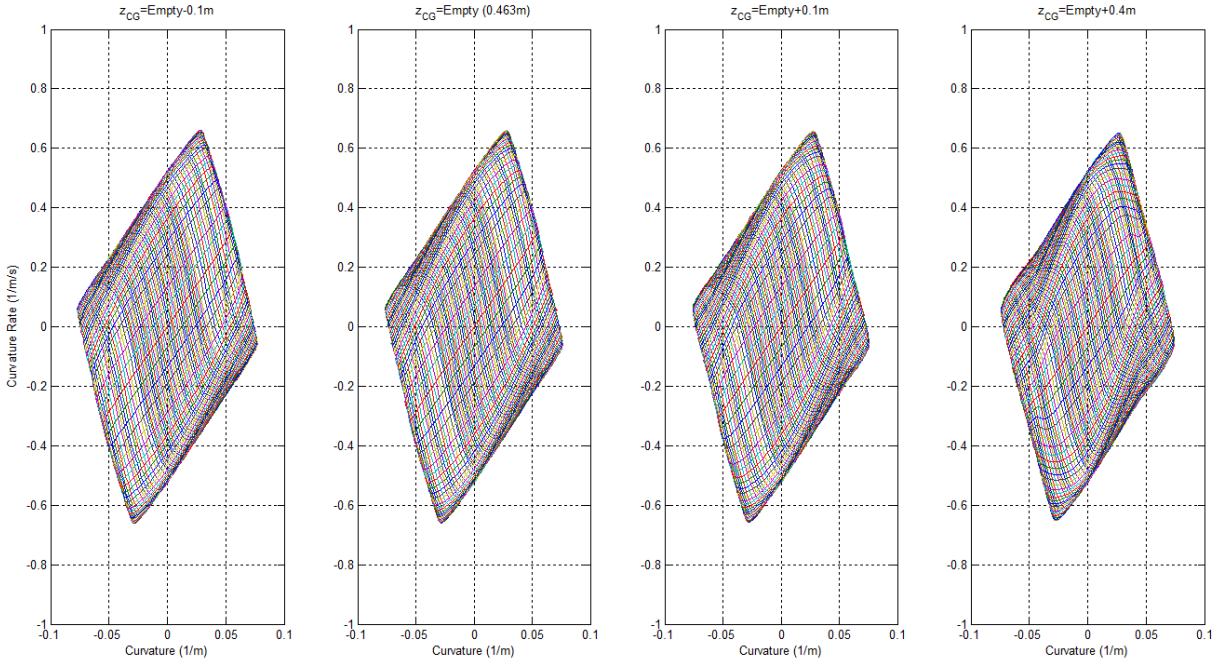

Fig. 8: *Plot of manuevering space diagrams showing the effect of variaiton of the z position of the CG. Note that the vehicle is largely insensitive to variation in this parameter in terms of manuevering space.*

The efficacy of the superposition technique for estimation of the resultant maneuvering space for variation in CG was tested by directly calculating force-moment diagrams for 294 differing

CG locations. These results were compared to the force-moment diagrams generated by the superposition technique. As can be seen from the example in Fig. 9, the directly calculated and superimposed diagrams are difficult to distinguish. The mean offsets for each of the 294 cases are plotted in Fig. 10. It can be seen from this figure that the error is a function of the absolute CG offset from the empty vehicle condition. It can be noted that the error in the non-dimensionalized coefficients is approximately an order of magnitude smaller than the maximum values of the coefficients. It follows that if the force-moment diagram shows a close correspondence, the maneuvering space generated from the diagram will have similar levels of error.

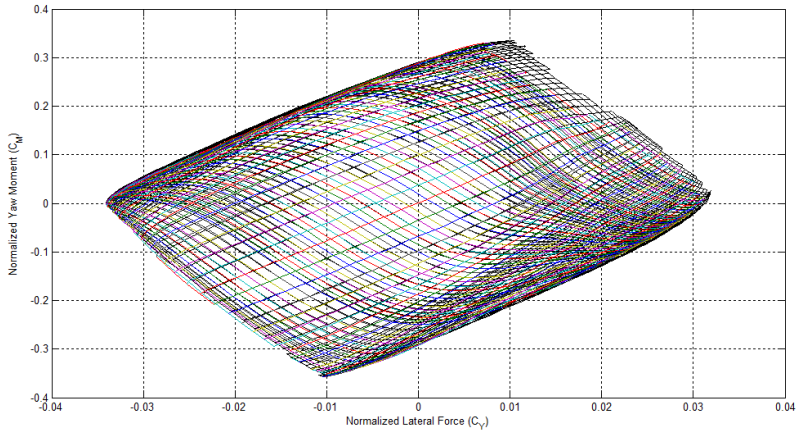

Fig. 9: *Plot of force-moment diagram for superimposed CG offsets (color) overlayed on directly calculated CG offset (black).*

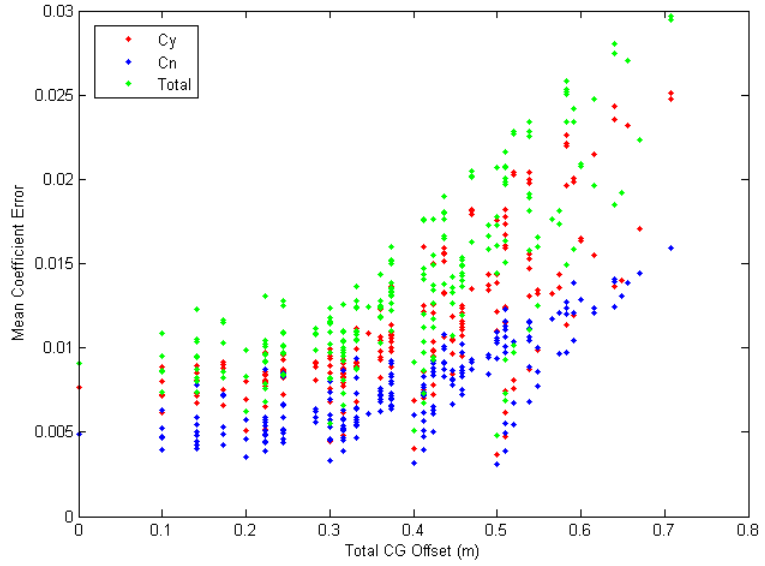

Fig. 10: *Plot error in superimposed forces and moments for varying absolute CG offsets.*

3.2 Coefficient of Friction and Acceleration Variation

The results of variation in the size of the maneuvering space as a result of changes in friction coefficient are shown in Fig. 11. As changing the coefficient of friction reduces the amount of overall force available, the resulting available curvature and curvature rate decrease dramatically with only about 15% of the dry road rate available on ice. This result should not be surprising, but it has great significance to the ability of motion planning algorithms to predict and execute available maneuvers. Due to the limited maneuverability on ice, these algorithms must plan appropriately and leave increased distance for desired maneuvers. Without knowledge of the available maneuvering space, this preplanning is unlikely to be successfully executed.

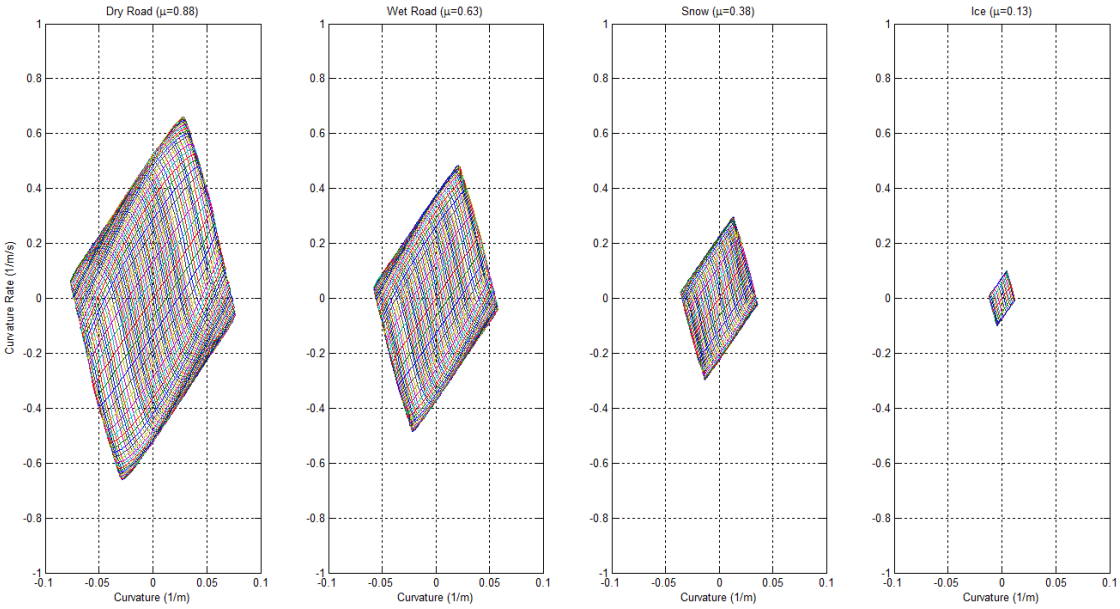

Fig. 11: *Plot of force-moment diagrams for varying values of coefficient of friction. Note the dramatic difference in the size of the total manuevering space and the corresponding limits of vehicle performance in terms of the motion variables.*

Longitudinal acceleration can also produce large changes in the available maneuvering space, as shown in Fig. 12. Heavy braking tends to compress the diagram into the understeering region, indicating that the front wheels are using most of the available force for braking and that the vehicle will skid before turning. This effect is also present in reduced form in the moderate braking case. The hard throttle case shows that the vehicle loses much of its ability to change paths quickly as the simulated vehicle lacks the power for power-on oversteer effects. Similarly to the coefficient of friction, these results indicate that it is necessary to account for the longitudinal acceleration when attempting to plan lateral maneuvers, particularly under hard braking when the vehicle is likely to skid.

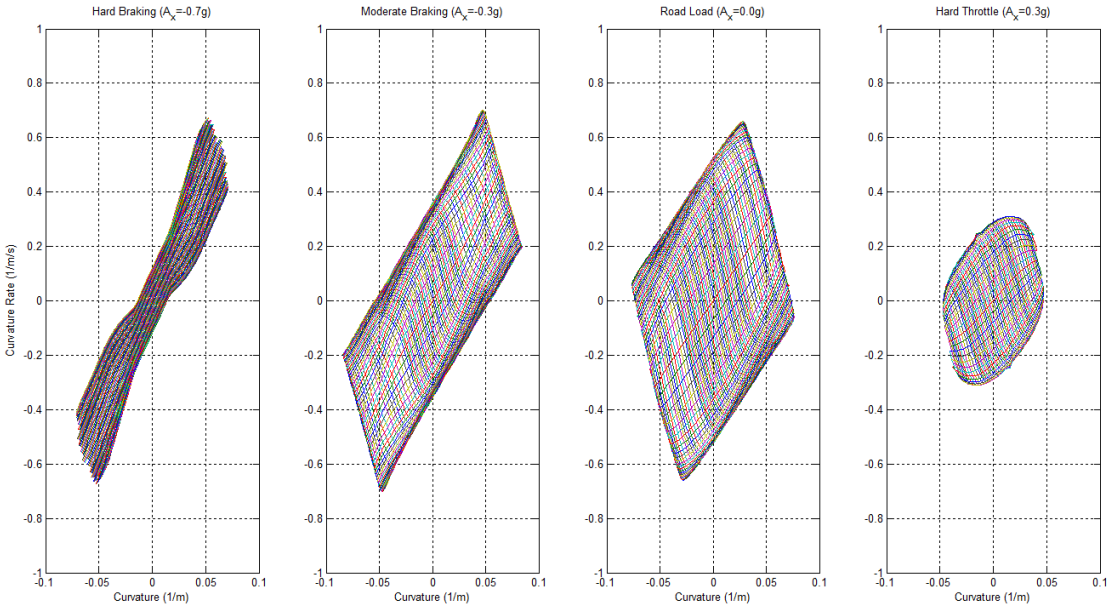

Fig. 12: *Plot of force-moment diagrams for varying values of longitudnal acceleration. Note the dramatic difference in the size and shape of the total manuevering space when the vehicle is at high throttle or heavy braking.*

4. Conclusions

The result of this work is a technique for estimating the available maneuvering space for a large mobile robot with varying load operating on varying terrain conditions. The technique relies on a precalculated force-moment representation to encode higher-order model characteristics in a form that can be accessed and processed in real-time to generate a searchable maneuvering space for autonomous controllers. Furthermore, a superposition-based technique can be used to allow for variations in load without unduly increasing the computational burden. Finally, it has been shown that the effects of changes in the ground-tire friction coefficient and longitudinal acceleration can be incorporated into this technique.

The results show that, at least in simulation, the force-moment technique can provide a reasonable approximation of vehicle motion while also demonstrating the importance of adapting the model to changes in CG location. The superposition technique appears to offer a good compromise between accuracy and computational tractability in accounting for changes in load state. It can also be seen from the results the vital importance of taking into account the coefficient of friction and longitudinal acceleration when attempting to estimate a maneuvering space and plan maneuvers.

To date, the results of this method have only been validated in simulation. Future testing on real vehicle hardware is needed to fully validate the ability of the proposed techniques to successfully predict maneuvering spaces. Unfortunately, the resources required for this type of testing are unavailable to the authors at the time of this writing and this validation must be left as future work.

The techniques developed in this paper offer the potential allow for real-time integration of adaptive models for feed-forward prediction of maneuvering spaces into autonomous controllers. This integration could greatly increase the safety and efficiency with which large mobile robots can operate in realistic conditions with realistic payloads.

5. Nomenclature

α_f Lateral slip angle of front wheels (rad)
α_r Lateral slip angle of rear wheels (rad)
δ Steering angle of front wheels (rad)
κ Path curvature (1/m)
$\dot{\kappa}$ Path curvature rate (1/m/s)
μ Friction coefficient
ϕ Roll rotation about *x*-axis (rad)
ψ Pitch rotation about *y*-axis (rad)
θ Yaw rotation about *z*-axis (rad)
$\dot{\theta}$ Yaw rate (rad/s)
$\ddot{\theta}$ Yaw acceleration (rad/s^2)
A_x Longitudinal acceleration (m/s^2)
C_α Overall cornering stiffness (N/rad)
C_M Yawing moment coefficient
C_{y_n} Lateral weight transfer coefficient for wheel *n*
C_Y Lateral force coefficient
DI Dynamic index
F_{x_n} Longitudinal force generated by wheel *n* (N)
F_{y_n} Lateral force generated by wheel *n* (N)
F_{z_n} Normal force at tire *n* (N)
g Acceleration due to gravity (m/s^2)
H Characteristic roll height (m)
I_z Yaw moment of inertia (kgm^2)
k_{ϕ_N} Effective roll stiffness of axle *N* (N/rad)
ℓ Wheelbase (m)
m_s Mass of sprung body (kg)
M Yawing moment (Nm)
p_n Position vector of wheel *n* from vehicle frame (m)
R_e Effective tire rolling radius (m)
S_n Slip ratio of tire *n*
V_x Longitudinal velocity (m/s)
W Vehicle weight (N)
ΔW_{x_N} Longitudinal weight transfer for axle *N* (N)
ΔW_{y_N} Lateral weight transfer for axle *N* (N)
x Longitudinal direction of vehicle frame (m)
x_{CG} Offset of CG from vehicle frame (m)
y Lateral direction of vehicle frame (m)

y_{CG} Offset of CG from vehicle frame (m)
Y Lateral force (N)
z Vertical direction of vehicle frame (m)
z_{CG} Offset of CG from vehicle frame in z-axis (m)

6. Acknowledgements

Acknowledgments are due to the members of my dissertation committee: Al Wicks, John Ferris, Dennis Hong, Sam Kherat, and Charles Reinholtz. I would also like to thank Ramadev Hukkeri for his technical assistance.

7. References

[1] C. Urmson, *et al*, "High speed navigation of unrehearsed terrain: Red team technology for grand challenge 2004," Robotics Institute, Carnegie Mellon University, Tech. Rep., 2004.

[2] C. Bottasso, et al, "Adaptive planning and tracking of trajectories for the simulation of maneuvers with multibody models," Computer Methods in Applied Mechanics and Engineering., vol. Computational Multibody Dynamics, pp. 7052–7072, 2006.

[3] R. Frezza, A. Beghi, and G. Notarstefano, "Almost kinematic reducibility of a car model with small lateral slip angle for control design," in Proc. IEEE International Symposium on Industrial Electronics ISIE 2005, vol. 1, 2005, pp. 343–348.

[4] J. Y. Wong, Theory of Ground Vehicles, 4th ed. Wiley, 2008.

[5] H. Abdellatif and B. Heimann, "Accurate modelling and identification of vehicle's nonlinear lateral dynamics," in Preprints of the 16th IFAC World Congress, 2005.

[6] E. Frazzoli, "Real-time motion planning for agile autonomous vehicles," in Proceedings of American Control Conference, 2001.

[7] A. Bacha, *et al*, "Odin: Team VictorTangos entry in the DARPA Urban Challenge," Journal of Field Robotics, vol. 25, no. 8, pp. 467–492, 2008.

[8] J.O. Hahn, R. Rajamani, and L. Alexander, "GPS-based real-time identification of tire-road friction coefficient," IEEE Transactions on Control Systems Technology, vol. 10, no. 3, pp. 331–343, 2002.

[9] S. Solmaz, M. Akar, R. Shorten, and J. Kalkkuhl, "Realtime multiple-model estimation of center of gravity position in automotive vehicles," Vehicle System Dynamics, vol. 46, pp. 763–788, 2008.

[10] T. A. Wenzel, K. J. Burnham, M. V. Blundell, and R. A. Williams, "Dual extended Kalman filter for vehicle state and parameter estimation," Vehicle System Dynamics, vol. 44, no. 2, pp. 153–171, 2006.

[11] J. Wang, L. Alexander, and R. Rajamani, "Friction estimation on highway vehicles using longitudinal measurements," Journal of Dynamic Systems, Measurement, and Control, vol. 126, pp. 265–275, June 2004.

[12] Y.H. J. Hsu, “Estimation and control of lateral tire forces using steering torque.” Ph.D. dissertation, Stanford University, 2009.

[13] Mechanical Simulation Corp., TruckSim Documentation, 8th ed., December 2009.

[14] W. Milliken and D. Milliken, Race Car Vehicle Dynamics. Warrendale, Pa.: SAE International, 1995.

[15] A. B.Will and S. H. Zak, “Modelling and control of an automated vehicle,” Vehicle System Dynamics, vol. 27:3, pp. 131–155, 1997.

[16] H. B. Pacejka, Tire and Vehicle Dynamics, 2nd ed. SAE International, 2006.

[17] T. A. Wenzel, “State and parameter estimation for vehicle dynamic control,” Ph.D. dissertation, Coventry University, UK, 2005, British Libary Shelf number XN092803 DSC.

[18] P. Currier. A Method for Modeling and Prediction of Ground Vehicle Dynamics and Stability in Autonomous Systems. Ph.D. dissertation, Virginia Tech, 2011.